Oriented collagen fibers direct tumor cell intravasation

Weijing Han[a], Shaohua Chen[b], Wei Yuan[c], Qihui Fan[a], Jianxiang Tian[b], Xiaochen Wang[a], Longqing Chen[d], Xixiang Zhang[e], Weili Wei[e], Ruchuan Liu[f], Junle Qu[c], Yang Jiao[b], Robert H. Austin[g,c,1], and Liyu Liu[f,a,1]

[a]Key Laboratory of Soft Matter Physics, Institute of Physics, Chinese Academy of Sciences, Beijing, China 100190; [b]Materials Science and Engineering, Arizona State University, Tempe, AZ 85281; [c]Key Laboratory of Optoelectronic Devices and Systems of Ministry of Education and Guangdong Province, Shenzhen University, Shenzhen, China 518060; [d]Division of Physical Science and Engineering, King Abdullah University of Science & Technology, Thuwal, Saudi Arabia 23955-6900; [e]Innovative Drug Research Center, Chongqing University, Chongqing, China 401331; [f]College of Physics, Chongqing University, Chongqing, China 401331; and [g]Department of Physics, Princeton University, Princeton, NJ 08544

Contributed by Robert H. Austin, July 28, 2016 (sent for review November 17, 2015; reviewed by Pascal Silberzan, Denis Wirtz, and Clare C. Yu)

In this work, we constructed a Collagen I–Matrigel composite extracellular matrix (ECM). The composite ECM was used to determine the influence of the local collagen fiber orientation on the collective intravasation ability of tumor cells. We found that the local fiber alignment enhanced cell–ECM interactions. Specifically, metastatic MDA-MB-231 breast cancer cells followed the local fiber alignment direction during the intravasation into rigid Matrigel (~10 mg/mL protein concentration).

cancer | intravasation | collagen | oriented invasion | microenvironment

Metastasis is a lethal milestone in cancer: Cells escape from the confinement of primary tumor sites (intravasation), invade tissues as well as the lymphatic and vascular systems, and finally colonize (extravasation) distant sites. It has been estimated that less than 1% of tumor cells undergo this process, but metastasis contributes to more than 90% of cancer-related deaths (1, 2). Metastasis involves both genetic and epigenetic alternation of tumor cells, as well as external biochemical and biophysical microenvironments (3–5). Pathology studies suggest that metastatic tumor cells exhibit highly branched morphologies and distinct aligned registration with aligned extracellular matrix (ECM) during metastatic tumor progression (4, 5).

We address three important questions concerning metastasis. (*i*) Can we build in vitro complex ECM structures with heterogeneously oriented collagen fibers and basement membrane components to mimic the cancer cell intravasation process? (*ii*) How does aligned collagen influence cell intravasation into/through the basement membrane before entering vessels? (*iii*) After cell detachment from the primary tumor site, how does a heterogeneous ECM with a varying degree of local fiber alignment influence cell intravasation and subsequent penetration into the basement membrane during their intravasation process? The major obstacle to addressing these questions is the difficulty in constructing both an in vitro 3D microenvironment to mimic the above process and flexible controls of the environmental parameters, such as fiber orientations in a complex collagen/Matrigel composite, nutrition, oxygen, drug concentrations, etc.

In breast cancer metastasis, cancer cells are believed to reorganize and progress through the interstitial ECM matrix, break through the basement membrane, and enter blood vessels or lymphatic capillaries (6–10). Fig. 1*C* presents a schematic illustration of the intravasation process in metastasis. Tumor-associated collagen signatures (TACS), basically environmentally elevated collagen density and collagen fiber reorganization, are used to stage mammary carcinoma tumor progression levels (6, 11–13). Fig. 1 presents hematoxylin/eosin (H&E)-stained biopsy slices of breast cancer imaged by second harmonic generation (SHG) under a two-photon confocal microscopy (A1R MP; Nikon) (detailed information provided in *SI Appendix, SI Text*) (6, 14, 15). Fig. 1 *A*, *1–3* shows the stained human invasive ductal carcinoma tumor at grade I. In the enlarged figures (Fig. 1 *A*, *2* and *3*), the cells have well-defined borders between the epithelium (gray) and stromal collagen (blue). The collagen fibers with higher density surrounding the tumor lesion are parallel to the tumor boundary, where the collagen is located but without obviously specific alignment (termed TACS-1) (12). Fig. 1 *B*, *1–3* represents invasive ductal carcinoma at grade III. In this case, after cell development, collagen fiber (blue) and tumor cells (gray) have more mixed forms. Clearly, the filament-like collagen fibers show macro alignment along the cell invasive directions (termed TACS-3) (12), which is believed to correlate with cell invasive potential in human tissues.

Recently, a number of mouse models and in vitro 3D cell culture systems have been used to study the cell underlying molecular and mechanical mechanisms for local collagen fiber reorganization and alignment. These experiments showed that epithelial cells and fibroblasts are capable of using associated proteins to initiate the Rho- and Rho kinase (Rock) pathway and then mediate actin-myosin contractility to orient collagen fibers (13, 16–18). However, it remains difficult to analyze the influences of the reorganized collagen tissue on tumor cells so far. The reason for that is mainly because precise quantification of reorganized collagen tissue in vivo is significantly restricted by existing methods. Therefore, in vitro 3D models have been constructed to build linear oriented matrices in microchannels by mechanical strain and have demonstrated that 3D matrix alignment facilitates persistent migration of tumor cells (9, 19–22). For example, Jimenez Valencia et al. studied cell behaviors in and around spheroids, which could be regarded as a tumor model at an early stage of the intravasation process. The analysis showed that the cells aligned perpendicularly to the spheroid surface due to applied traction forces from the cells in the spheroid to reorganize the collagen matrix (23). Although the density and alignment of fibrillary collagen are clearly important markers in diagnosing a human breast carcinoma's stage (12, 14), biopsies merely provide static "snapshots" of the morphology

Significance

Intravasation is an early stage of metastasis that involves metastatic cells moving from the tumor into the extracellular matrix (ECM), breakthrough of the basement membrane, and entry into blood vessels. We found that the oriented fibers greatly enhance and facilitate the metastatic cell intravasation process during metastasis. We suggest that a possible "tissue treatment" therapy could be considered, in which the ECM fiber structure orientation in the tumor microenvironment might be altered to minimize the intravasation rate of metastatic cells.

Author contributions: W.H., S.C., W.Y., Q.F., X.W., L.C., X.Z., J.Q., Y.J., and L.L. designed research; W.H., S.C., W.Y., Q.F., J.T., X.W., L.C., X.Z., and L.L. performed research; W.H., S.C., W.Y., Q.F., J.T., X.W., L.C., X.Z., J.Q., Y.J., R.H.A., and L.L. analyzed data; and W.W., R.L., Y.J., R.H.A., and L.L. wrote the paper.

Reviewers: P.S., Institut Curie-Centre de Recherche; D.W., The Johns Hopkins University; and C.C.Y., University of California, Irvine.

The authors declare no conflict of interest.

[1]To whom correspondence may be addressed. Email: lyliu@cqu.edu.cn or austin@princeton.edu.

This article contains supporting information online at www.pnas.org/lookup/suppl/doi:10.1073/pnas.1610347113/-/DCSupplemental.

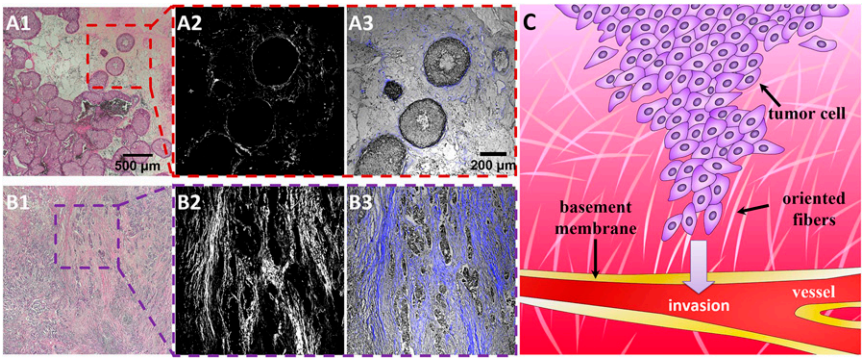

Fig. 1. Clinic biopsy of breast carcinoma progression at early (TACS-1) and late (TACS-3) stages. (*A*, *1–3*) show the H&E-stained slices of tumor cell development during the TACS-1 stage. (*A*, *2*) A second harmonic generation (SHG) image illustrating the complexity and variability of collagen localization. Combined with bright-field cell images, it seems that the locally dense collagen matrix surrounds ducts with a spherical morphology. For TACS-3 (*B*, *1–3*), the tumor cells (gray color in *B*, *3*) seem to interact with the parallel aligned collagen fibers for their invasion. (*C*) Drawing illustrating that metastatic tumor cells interact with oriented ECM fibers and invade toward the basement membrane and vessels during the intravasation process. The color depth represents the nutrient gradient in the tissues; higher nutrition in vessels is an attraction for cell intravasation into tissues.

of cells and collagen fibers. Further, although there have been constructs of homogeneous localized collagen alignments and of systematic quantified fiber alignment and associated cell displacement (9), a basic in vitro 3D ECM model for intravasation study should at least include structures mimicking both the interstitial matrix (collagen) and basement membrane (Matrigel), with various degrees of heterogeneities (e.g., locally oriented Collagen I fibers).

Materials and Methods

To investigate the effects of collagen alignment on the intravasation process, we created an engineered microenvironment within a microfabricated chip, using layered Collagen I and Matrigel with controllable heterogeneities in in vitro intravasation studies, as shown in Fig. 2*A*. The heterogeneous landscape is constructed within a microfabricated chip, shown in Fig. 2. The pillar-like inner structures would efficiently stabilize gel structures inside and avoid unflavored mechanical influence by the fluid at the side channels (24).

Matrigel (100% concentration, 356237; Corning) and Collagen I (2 mg/mL in water, 354236; Corning) created the sandwiched ECM. The heterogeneous Collagen I orientation was induced by internally developing strain fields due to the Matrigel volume swelling upon setting (25–29). Fig. 2*B* shows the heterogeneous microenvironment made of the mechanically organized Collagen I–Matrigel composite structure (sandwiched ECM). Collagen I was injected while fluid into the Matrigel (Fig. 2 *C*, *1* and *2*). During the composite ECM solidification, the Matrigel volume expanded while the Collagen I section shrank (*SI Appendix*, Figs. S11 and S12). Although the ECM interface was reshaped, Fig. 2 *C*, *3* shows using cryo-Scanning Electron Microscope (FESEM, SU8010; Hitachi) imaging that the interface still remained distinct, indicating that Collagen I and Matrigel had little to no diffusion or mixing at the interface. Detailed information is provided in *SI Appendix*, *SI Text*.

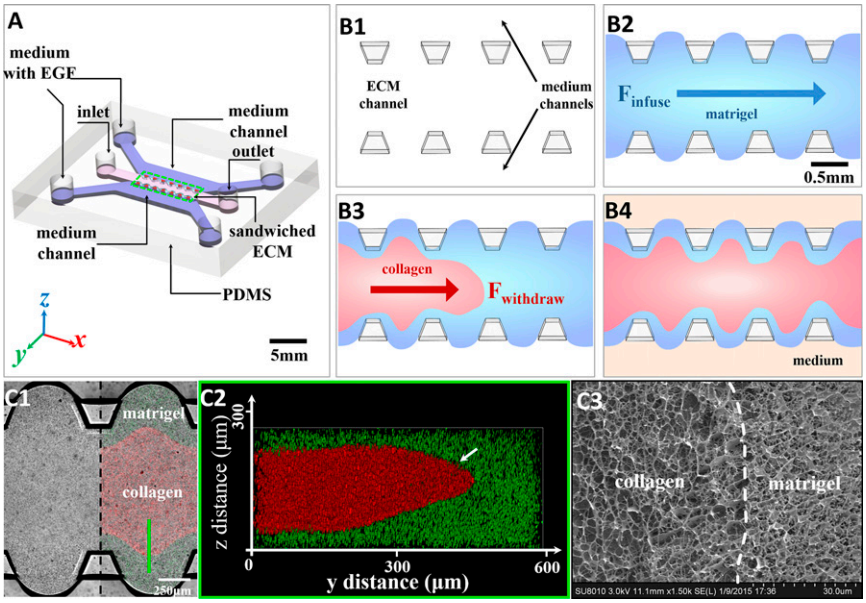

Fig. 2. The formation of the sandwiched ECM in the microfluidic device and the ECM structure characterization. (*A*) Diagram of the polydimethylsiloxane (PDMS)-based microfluidic chip. The core consists of a 3D sandwiched ECM in the center, shouldered by two medium channels of medium with EGF. (*B*, *1–4*) The formation process of the sandwiched ECM. First, the liquid Matrigel (blue) was injected into the ECM channel (*B*, *2*). Then the liquid collagen gel (red) substituted for the Matrigel in the middle part by negative pressure from the outlet (*B*, *3*). After injection, the sandwiched ECM was cured at 37 °C for 30 min before the side channels were filled with medium (*B*, *4*). (*C*, *1–3*) The characterization of the sandwiched ECM in the microfluidic device. The confocal microscopy shows the planar view (*C*, *1*) and z-stack images (*C*, *2*) of the sandwiched gel. Imaging using a cryo-SEM figure (*C*, *3*) shows the Collagen I–Matrigel interface in the sandwiched ECM, which indicates that the initial collagen–Matrigel matrices had a distinct interface without obvious fusion.

To identify the interface reshaping the Collagen I matrix section, fluorescent and reflection modes (30) of the confocal microscopy were used to characterize the Collagen I (blue region) and the Matrigel (mixed with green fluorescent beads) regions, respectively. Fig. 3*A* is a top view of the 3D reconstruction images on the composite ECM region and shows that Collagen I fibers form peninsula-like protrusions with significant perpendicular orientation at the tips after 24 h. In the 3D image reconstruction, images of green fluorescent beads in Matrigel layers do not overlap with Collagen I. Fig. 3*B* shows the corresponding 3D profiles in the vertical direction (*z* axis). Collagen I fibers connected with Matrigel were significantly reorganized and reoriented after being squeezed by Matrigel swelling from the top and bottom sides (*SI Appendix*, Fig. S9*C*). Fig. 3 *C*, *1* and *C*, *2* shows the detailed fiber morphology at the Collagen I–Matrigel boundary (red boxed region) as well in the bottom Collagen I region (green boxed region). Fig. 3 *C*, *1* shows that the fibers realigned in regular patterns and were perpendicular to the interface. The length of the longest visible fiber was about 30 μm. This observation implies that the collagen fibers have possibly infiltrated the Matrigel. The fiber density increased at the Collagen I bottom region (Fig. 3 *C*, *2*). For comparison, Fig. 3 *C*, *3* shows the control experiment of pure and homogenous Collagen I at the same concentration with random fiber orientation.

The Curvelet-Based Alignment Analysis software (University of Wisconsin at Madison) was used to quantitatively analyze the Collagen I fiber orientation (Fig. 3 *C*, *1* and *2*) in sandwiched ECM and pure Collagen I in the control experiment (Fig. 3 *C*, *3*). Fiber orientation was quantified by measuring its angle relative to the channel direction (*x* axis), and angle frequency was plotted as a function of its distribution. Each bar represents the angle frequency within ± 2.5°. In Fig. 3 *D*, *1*, the analysis shows that the majority of fibers in the protrusion tip region were oriented along the vertical direction toward the Matrigel region. However, in the Collagen I bottom region (Fig. 3 *D*, *2*), the majority of the fibers were oriented in a wide distribution centered at 0°, possessing on average parallel orientations to the ECM channel. In the control experiment, the same analysis on the pure Collagen I showed random orientation of the fibers (Fig. 3 *D*, *3*). A complete landscape of the distribution of collagen fiber orientation is plotted as a function of the position of collagen fiber in the sandwiched ECM in *SI Appendix*, Fig. S10.

In our system, the formation of the oriented collagen fiber landscape was controlled by the internal strain field inside the composite gels during the sandwiched ECM injection and Matrigel squeezing process. First, the injection of liquid Collagen I into viscous liquid Matrigel led to external forces that constrained the macroscopic shape of the Collagen I fiber network during gelation (31, 32). Further, the swelling Matrigel anisotropically squeezed specific Collagen I regions after immersion in the culture medium, leading to further fiber reorientation and reorganization.

To verify this scenario, we used a confocal microscope to take time-lapse images of the displacements of fluorescent beads in the composite ECM for 300 min continuously after immersion in culture medium. The tracked traces of the red fluorescent beads indicated their spatial movements in Collagen I region, and the yellow green fluorescent beads provided directions and degrees of the Matrigel deformation. The continuous tracking data were analyzed using the software Imaris (Bitplane), and the spatial displacements of the beads were plotted as a function of time, as shown in Fig. 4*A*. The *z* axis sectional view of displacement (Fig. 4*A*) during the tracking process indicates that the displacements of fluorescent microspheres in Collagen I were mainly constrained in the *y*–*z* plane and pointed to the center of the ECM channel. Our result indicates that the strain field in the latter process had major contributions to the heterogeneous collagen fiber reorientations (*SI Appendix*, Figs. S12 and S13).

The displacement field obtained via bead tracking was used to estimate the stress field in the system. In our analysis, elasticity was assumed for both Collagen I and Matrigel. Although both materials may exhibit certain viscoelastic behavior, we expected the estimated stress field qualitatively to represent the actual stress field in the system. Because the Collagen I section and the inside fiber orientation was our primary concern, its confocal image was reconstructed in 3D and subsequently used to analyze the stress inside. Our analysis indicated that σ_x, σ_y and τ_{yz} have major contributions to fiber orientation distribution (complete analysis of the strains provided in *SI Appendix, Stress Field in Collagen I and Matrigel*) (*SI Appendix*, Fig. S2). The normal stress σ_y was mainly due to the resistance of Matrigel to the intrusion of Collagen I, and the shear stress τ_{xy} and τ_{xz} fluctuated around zero. Therefore, these stress components did not significantly contribute to the observed fiber orientation correlations. As shown in Fig. 4 (*SI Appendix*, Movie S1), it could be clearly seen that, close to the Collagen I–Matrigel interface (i.e., the extruded border of Collagen I shown in Fig. 4 *C* and *D*), the system is under biaxial compression. This stress state could be understood as follows: In response

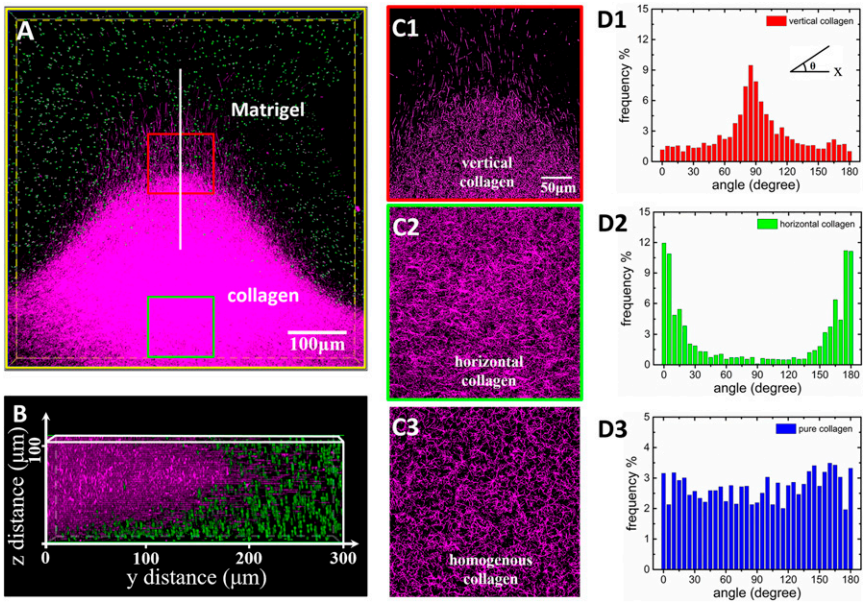

Fig. 3. Analysis of collagen fiber orientation in the sandwiched ECM after formation. (*A*) The 3D confocal image reconstruction via image stacking (top view) shows the Matrigel/collagen composite ECM and their interface in three dimensions. (*B*) The cross-sectional view (side view) of the 3D ECM shows that the Matrigel affected the local morphology of collagen In the interface region. (*C*, *1*) The collagen fibers near the interface region possess vertical orientations (red box). (*C*, *2*) The collagen fibers in the centered region possess horizontal orientations (green box). Correspondingly, *D*, *1* and *2* demonstrates the orientation distribution analysis of the collagen fibers in the "vertical" and "horizontal" regions, respectively. The angle of fiber orientation is defined as the *Inset* in *D*, *1*. As a comparison, *C*, *3* and *D*, *3* show the collagen fiber organization and orientation distribution in pure collagen as the control experiment. The quantitative analysis of the fiber orientation in the vertical region yielded a strong peak around 90° perpendicular to the ECM interface whereas the fiber orientation distribution in the horizontal region possesses peaks around 0°. The fibers in the pure collagen were randomly oriented and possessed a uniform distribution of angles.

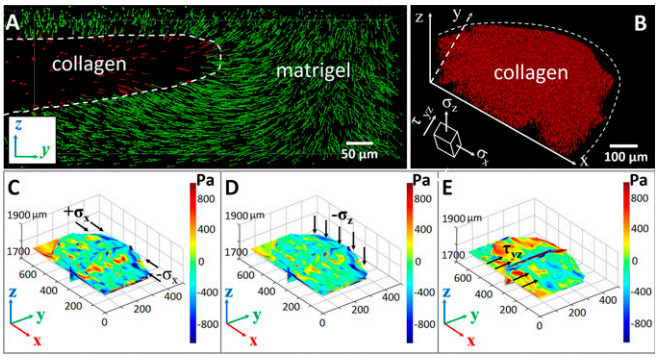

Fig. 4. Dynamic strain field and analysis in the ECM. (*A*) Displacement field of fluorescent beads imbedded inside the collagen (red) and Matrigel (green). (*B*) A 3D reconstructed image of the beads' spatial distribution in the collagen region, with an illustration of action directions of different stress components. (*C*–*E*) The stress components σ_x, σ_z, and τ_{yz} in collagen. The results showed that large compressive normal stresses σ_x and σ_z led to a strong biaxial stress state and thus caused the reorientation of collagen fibers along the *y* direction in regions close to the extrusion front. The large shear stress τ_{yz}, induced by the relative motion of two successive thin layers of collagen parallel to the *y*–*z* plane, could lead to significant fiber rotation and, thus, fiber realignment along the *x* direction.

to the osmotic pressure and Matrigel volume swelling, the convex extrusion front of Collagen I was "squeezed," leading to large compressive normal stress σ_x and σ_z. Such strong biaxial stresses caused the reorientation and local alignment of collagen fibers along the *y* direction in regions close to the extrusion front, which is consistent with the quantitative analysis of the confocal micrographs (Fig. 3 *C*, *1*). In the middle region of the Collagen I system that was analyzed previously, both the normal and shear stresses fluctuated and thus could not lead to significant alignment of the Collagen I fibers. This result was consistent with the low degree of orientation correlations among the fibers observed in the confocal micrograph. On the hand, a large shear stress τ_{yz} was observed at the bottom of the Collagen I region we analyzed (Fig. 4*E*). As the Collagen I region close to the extrusion front was squeezed to the middle, the Collagen I away from the front was also "dragged" to the middle, leading to the observed large shear stress τ_{yz} (Fig. 4*E*). Such a shear stress, which could be considered as caused by the relative motion of two successive thin layers of Collagen I parallel to the *y*–*z* plane, could lead to significant fiber rotation and thus alignment along the *x* direction, which is consistent with the strong fiber alignment in the horizontal direction observed in the confocal micrograph (Fig. 3 *C*, *2*).

Results and Discussion

Cell Behavior Heterogeneity of MDA-MB-231 Cells in the Composite ECM. Metastatic breast cancer cells (MDA-MB-231) (Xiehe Medical University Cell Culture Center) were mixed with the Collagen I and injected inside the chip with the collagen. They were used to characterize the influences of oriented collagen on collective cell invasive behavior. The orientation of MDA-MB-231 cells inside the ECM was quantified by ImageJ and then displayed as population distributions of the measured angles. Because cell nucleus shape mostly represents its morphological change (33–35), the MDA-MB-231 cells were stained with Hoechst so that their nuclei would be visible under the confocal microscopy.

Fig. 5*A* presents the integration of the bright-field and fluorescent images of cells at 96 h. The blue color indicates the nucleus position. The cells in the Collagen I region exhibited a highly heterogeneous orientation. Fig. 5 *B*, *1–3* shows the enlarged bright-field images of the boxed regions shown in Fig. 5*A*. Fig. 5 *C*, *1–3* presents the fluorescence images of cell nucleus orientations. In particular, Fig. 5 *B*, *1* and *C*, *1* shows that, inside the tip regions, the cell morphology and nucleus shape revealed that MDA-MB-231 cells assumed a vertical orientation through the ECM interface. Behind the tip zone, the yellow boxed region shows that the distribution of tumor cell orientation was gradually changed from the vertical direction to a random orientation (Fig. 5 *B*, *2* and *C*, *2*). Meanwhile, in the middle region of Collagen I, the cells presented a horizontal orientation (Fig. 5 *B*, *3* and *C*, *3*).

The distributions of tumor cell orientation in different regions were analyzed using Curvelet-Based Alignment Analysis software and plotted as population distributions of the measured angles. In the tip zone, tumor cells formed cell branches, and there were more than 25% of tumor cells possessing orientations distributed around 90° (Fig. 5 *D*, *1*). The cells around the ECM interface region (yellow box) exhibited almost uniform angular distribution (Fig. 5 *D*, *2*). The orientations of cells in the middle region were mostly distributed around 0° and 180° (Fig. 5 *D*, *3*). These results show that the cell orientation distribution was highly consistent with the distribution of Collagen I fiber orientation in the composite ECM. On the other hand, in the control experiment with pure and homogenous Collagen I (*SI Appendix*, Fig. S13), MDA-MB-231 cells had a random orientation distribution (detailed information provided in *SI Appendix*, *SI Text*). This observation indicates that the composite heterogeneous ECM had strong guidance for the orientation of MDA-MB-231 cells via the locally reorganized Collagen I fibers.

Enhanced MDA-MB-231 Cell Intravasation into the Matrigel Region. Fig. 6 *A*, *1–3* presents bright-field pictures taken by confocal microcopy and show the MDA-MB-231 cell intravasation toward the Matrigel region with time. Fig. 6 *B*, *1–3* shows the fluorescence images showing the relative positions of the invading cells within the ECM network. At 0 h, MDA-MB-231 cells were distributed randomly in the Collagen I region, most of which were more than 100 μm away from the ECM interface (indicated by the green fluorescent beads). After 48 h, the cells moved toward the interface with significantly increased cell numbers due to rapid cell proliferation. Some cells, as indicated by the arrow, already had a vertical orientation approach and had begun to enter the interface (Fig. 6 *B*, *2*). After 96 h, the Collagen I shrinkage continued and significantly drove the gel interface to the center. However, the pioneering cell still invaded more than 200 μm deep into the Matrigel (100% concentration) region, as indicated by the white arrow in Fig. 6 *B*, *3*). The major cell intravasation exhibited a collective behavior in the form of "single stream" branches (36). The cell intravasation speed was about 3 μm/h. Note that the

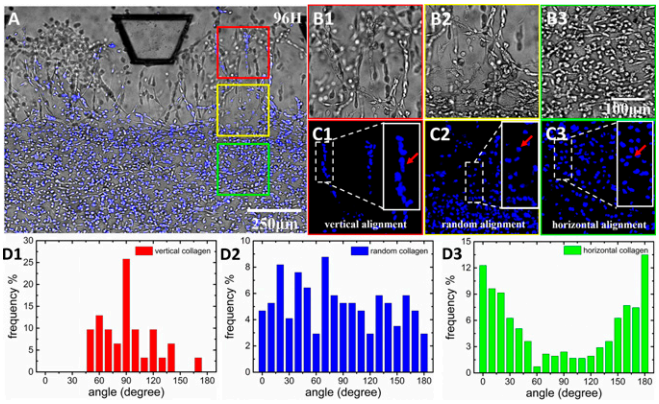

Fig. 5. Tumor cell in vitro intravasation in the heterogeneous ECM with various degree of local collagen fiber alignment. (*A*) The distribution of invading tumor cells in the sandwiched ECM after 96 h (*B*, *1–3* and *C*, *1–3*). Enlarged *Insets* respectively show the bright field and fluorescent images of the spatial distribution and morphology of cells invading in the Matrigel region (*B*, *1* and *C*, *1*), the aligned collagen region (*B*, *2* and *C*, *2*), and the randomly oriented collagen region (*B*, *3* and *C*, *3*). The *Insets* in *C*, *1–3* illustrate the magnifications of the corresponding areas, representing alignments of the cell nucleus (vertical, random, and horizontal alignment, as indicated by arrows). (*D*, *1–3*) The quantitative analysis of cell orientation distributions in the aforementioned corresponding regions.

Collagen I fibers and the orientation became indistinct under the reflection mode of confocal microscopy (indicated by the yellow arrow in Fig. 6 *B*, *3*), which suggests that the Collagen I fiber network was remodeled during the cell intravasation. In this process, the cancer cell should express matrix metalloproteinases (MMPs) that degrade the ECM, generate local paths, and help the cell invasion (37). At the 144th hour (Fig. 6*C*), the front cells successfully crossed the entire Matrigel region, which suggests that, even if there may be some infiltration of the collagen fibers in the Matrigel, the influence goes much further than their penetration lengths because cells could travel a much longer distance in the Matrigel after passing the interface. As a control, in homogeneous collagen, MDA-MB-231 were unable to invade the Matrigel (see *SI Appendix*, *Cell Invasion Process from Homogeneous Collagen to Matrigel* and *SI Appendix*, Fig. S1).

Weak Intravasation of MCF-7 Cells in the Heterogeneous ECM. In the control experiment, weakly metastatic breast cancer cell line MCF-7 cells (Xiehe Medical University Cell Culture Center) were also cultured in the composite ECM structures (Fig. 7). The MCF-7 cells exhibited spherical morphologies and more proliferation than intravasation. After 168 h, the cells aggregated and formed spheroid-like structures, which did not exhibit obvious intravasation into the Matrigel region. This result indicates that MCF-7 cells are unable to acquire enhanced invasive potentials from the prealigned Collagen I fibers. It would seem that metastatic cancer cells (such as MDA-MB-231 cells) are more sensitive to an orientated collagen fiber environment, which may benefit and enhance cell invasive potentials along the intravasation process. Opposite to that, the same environment would not affect the intravasation of weak metastatic cells (such as MCF-7 cells).

Conclusions

Our analysis and results show that the orientation of the Collagen I matrix can lead to significantly enhanced tumor metastatic potential. To further elucidate possible mechanisms for the enhanced intravasation, we used a minimalist 3D cell migration model that incorporates the effects of both a collagen network microstructure and a local fiber stress state on cell migration (see *SI Appendix*, *Computational Model for 3D Single Cell Migration in ECM*) without explicitly considering the effects of chemotactic cues. Specifically, we considered polarized actin polymerization (correlated with migration direction) and biased focal adhesion formation depending on the stress state of the fiber segments, leading to directed cell motions. On the other hand, the active contraction of actin filaments also generated forces on the fibers mechanically coupled to the cell cytoskeleton via focal adhesion sites, and the forces propagated via the fiber network to cells at distant locations. Our simulations suggest that an oriented fiber network could lead to much stronger migration persistence for individual cells due to contact guidance (*SI Appendix*, Figs. S3–S6) and to collective directional migration for multiple cells due to both contact guidance and mechanical regulation (*SI Appendix*, Figs. S7 and S8). The resulting highly directional migration persistence could be responsible for the large penetration depth (~200 μm) in the Matrigel (Fig. 6 *B*, *1–3*) and even the breakthrough (Fig. 6*C*). This depth is much larger than the thickness of the interface layer (~20 μm), suggesting that the cells acquire enhanced invasive potentials during the contact guidance or mechanical regulation.

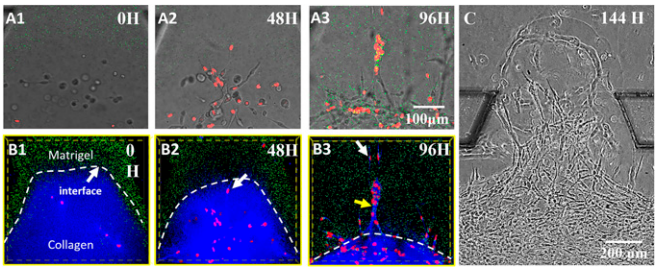

Fig. 6. The enhanced intravasation process of MDA-MB-231 cells in the composite ECM. (*A*, *1–3*) The bright-field images showing snapshots of invading cells taken every 48 h. (*B*, *1–3*) The fluorescent images combined with reflective mode, which show the Matrigel region with green beads embedded, the collagen region (blue), and the nuclei of invading cells (red). It is clear that, at the 96th hour, guided by oriented collagen fibers, the cells aggregated and strongly invaded into the rigid Matrigel region in single-stream forms. The field of view is the same for *A*, *1–3* and *B*, *1–3*. (*C*) Cells broke through the Matrigel region and reached the side channel at the 144th hour, indicating the long-distance influence of the collagen fibers in enhancing the intravasation process of MDA-MB-231.

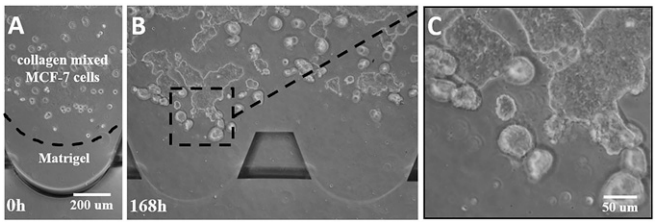

Fig. 7. Proliferation and intravasation of weak metastatic MCF-7 cells in the composite ECM at the 0 h (*A*) and 168th hour (*B*), respectively. The enlarged image (*C*) shows that the cells present weak invasive behaviors, with spherical and sheet-like morphology inside the collagen matrix.

It is known that radiotherapy, to some extent, promotes the specific alignment of the Collagen I matrix (38–41). Therefore, in light of our study, if there are tumor cells that have survived the treatment and proliferated after therapy, the oriented fiber network may drive their subsequent aggressive metastasis. We suggest that future therapy should consider treatment of the tumor physical microenvironment. The patients could receive a "tissue therapy" that alters the tumor microenvironment (e.g., to recover local ECM fiber orientation to the original unoriented state), to minimize the aggressive intravasation of the metastatic cancer cells. Some strategies have been developed to inhibit fiber formation and/or disassembly of the fibers: For example, physical (e.g., light, heat, and electrical field) (42–44) as well as chemical (45, 46) agents have been applied to this topic. Among the above methods, use of the nanomaterial graphene oxide to transform the energy of near infrared (NIR) light to thermal energy and consequently induce disassembly of the preformed fibers of the amyloid protein (47) might be applied using a spatiotemporal controllable photo-thermal treatment. We suggest that this approach seems most likely to match the concept of tissue therapy that we propose.

Our results provide strong evidence that, besides intrinsic properties such as genetics and morphology, the tumor microenvironment of local Collagen I fiber orientations plays an important role in guiding cell intravasation, promoting cell breakage into the basement membrane before entering the circulation systems. Our finding not only agrees with clinical biopsies of breast cancer metastatic cell intravasation, but also systematically reveals the process and mechanism of ECM enhanced cell intravasations during intravasation in a quantitative way. We propose that future therapy could consider tuning tumor biophysical microenvironment: e.g., recovering ECM fiber orientations and using local tissue treatment to reduce the intravasation potential of metastatic cancers.

ACKNOWLEDGMENTS. We thank our referees for provocative questions that greatly improved the paper. This work was supported by State Key Development Program for Basic Research of China Grant 2013CB837200, National Natural Science Foundation of China Grants 11474345 and 11274200, Beijing Natural Science Foundation Grant 7154221, National

Cancer Institute Grant U54CA143803, and Arizona State University start-up funds. The content is solely the responsibility of the authors and does not necessarily represent the official views of the National Cancer Institute or the National Institutes of Health.

1. Sleeman J, Steeg PS (2010) Cancer metastasis as a therapeutic target. *Eur J Cancer* 46(7):1177–1180.
2. Steeg PS, Theodorescu D (2008) Metastasis: A therapeutic target for cancer. *Nat Clin Pract Oncol* 5(4):206–219.
3. Fang M, Yuan J, Peng C, Li Y (2014) Collagen as a double-edged sword in tumor progression. *Tumour Biol* 35(4):2871–2882.
4. Gelain F, Bottai D, Vescovi A, Zhang S (2006) Designer self-assembling peptide nanofiber scaffolds for adult mouse neural stem cell 3-dimensional cultures. *PLoS One* 1(1):e119.
5. Xu J, et al. (2001) Proteolytic exposure of a cryptic site within collagen type IV is required for angiogenesis and tumor growth in vivo. *J Cell Biol* 154(5):1069–1079.
6. Dang TT, Prechtl AM, Pearson GW (2011) Breast cancer subtype-specific interactions with the microenvironment dictate mechanisms of invasion. *Cancer Res* 71(21): 6857–6866.
7. Cil T, et al. (2009) Mammographic density and the risk of breast cancer recurrence after breast-conserving surgery. *Cancer* 115(24):5780–5787.
8. Gilkes DM, et al. (2013) Collagen prolyl hydroxylases are essential for breast cancer metastasis. *Cancer Res* 73(11):3285–3296.
9. Martin LJ, Boyd NF (2008) Mammographic density. Potential mechanisms of breast cancer risk associated with mammographic density: Hypotheses based on epidemiological evidence. *Breast Cancer Res* 10(1):201.
10. Riching KM, et al. (2014) 3D collagen alignment limits protrusions to enhance breast cancer cell persistence. *Biophys J* 107(11):2546–2558.
11. Schedin P, Keely PJ (2011) Mammary gland ECM remodeling, stiffness, and mechanosignaling in normal development and tumor progression. *Cold Spring Harb Perspect Biol* 3(1):a003228.
12. Bredfeldt JS, et al. (2014) Automated quantification of aligned collagen for human breast carcinoma prognosis. *J Pathol Inform* 5(1):28.
13. Conklin MW, et al. (2011) Aligned collagen is a prognostic signature for survival in human breast carcinoma. *Am J Pathol* 178(3):1221–1232.
14. Keikhosravi A, Bredfeldt JS, Sagar AK, Eliceiri KW (2014) Second-harmonic generation imaging of cancer. *Methods Cell Biol* 123:531–546.
15. Perry SW, Burke RM, Brown EB (2012) Two-photon and second harmonic microscopy in clinical and translational cancer research. *Ann Biomed Eng* 40(2):277–291.
16. Provenzano PP, et al. (2008) Nonlinear optical imaging of cellular processes in breast cancer. *Microsc Microanal* 14(6):532–548.
17. Goetz JG, et al. (2011) Biomechanical remodeling of the microenvironment by stromal caveolin-1 favors tumor invasion and metastasis. *Cell* 146(1):148–163.
18. Provenzano PP, et al. (2006) Collagen reorganization at the tumor-stromal interface facilitates local invasion. *BMC Med* 4(1):38.
19. Provenzano PP, et al. (2008) Collagen density promotes mammary tumor initiation and progression. *BMC Med* 6(1):11.
20. Carey SP, Starchenko A, McGregor AL, Reinhart-King CA (2013) Leading malignant cells initiate collective epithelial cell invasion in a three-dimensional heterotypic tumor spheroid model. *Clin Exp Metastasis* 30(5):615–630.
21. Provenzano PP, Inman DR, Eliceiri KW, Trier SM, Keely PJ (2008) Contact guidance mediated three-dimensional cell migration is regulated by Rho/ROCK-dependent matrix reorganization. *Biophys J* 95(11):5374–5384.
22. Vader D, Kabla A, Weitz D, Mahadevan L (2009) Strain-induced alignment in collagen gels. *PLoS One* 4(6):e5902.
23. Jimenez Valencia AM, et al. (2015) Collective cancer cell invasion induced by coordinated contractile stresses. *Oncotarget* 6(41):43438–43451.
24. Wang H, Abhilash AS, Chen CS, Wells RG, Shenoy VB (2014) Long-range force transmission in fibrous matrices enabled by tension-driven alignment of fibers. *Biophys J* 107(11):2592–2603.
25. Zervantonakis IK, et al. (2012) Three-dimensional microfluidic model for tumor cell intravasation and endothelial barrier function. *Proc Natl Acad Sci USA* 109(34): 13515–13520.
26. Anseth KS, Bowman CN, Brannon-Peppas L (1996) Mechanical properties of hydrogels and their experimental determination. *Biomaterials* 17(17):1647–1657.
27. Drury JL, Mooney DJ (2003) Hydrogels for tissue engineering: Scaffold design variables and applications. *Biomaterials* 24(24):4337–4351.
28. Lu K (2011) Modelling of multicomponent diffusion and swelling in protein gels. PhD thesis (University of Canterbury, Christchurch, New Zealand).
29. Lucantonio A, Nardinocchi P, Teresi L (2013) Transient analysis of swelling-induced large deformations in polymer gels. *J Mech Phys Solids* 61(1):205–218.
30. Raeber GP, Lutolf MP, Hubbell JA (2005) Molecularly engineered PEG hydrogels: A novel model system for proteolytically mediated cell migration. *Biophys J* 89(2):1374–1388.
31. Brightman AO, et al. (2000) Time-lapse confocal reflection microscopy of collagen fibrillogenesis and extracellular matrix assembly in vitro. *Biopolymers* 54(3):222–234.
32. Knapp DM, et al. (1997) Rheology of reconstituted type I collagen gel in confined compression. *J Rheol (NYNY)* 41(5):971–993.
33. Lii J, et al. (2008) Real-time microfluidic system for studying mammalian cells in 3D microenvironments. *Anal Chem* 80(10):3640–3647.
34. McKee CT, Raghunathan VK, Nealey PF, Russell P, Murphy CJ (2011) Topographic modulation of the orientation and shape of cell nuclei and their influence on the measured elastic modulus of epithelial cells. *Biophys J* 101(9):2139–2146.
35. Versaevel M, Grevesse T, Gabriele S (2012) Spatial coordination between cell and nuclear shape within micropatterned endothelial cells. *Nat Commun* 3:671.
36. Zhao X, Chen H, Liu X, Cang J (2013) Orientation-selective responses in the mouse lateral geniculate nucleus. *J Neurosci* 33(31):12751–12763.
37. Friedl P, Bröcker E-B (2000) The biology of cell locomotion within three-dimensional extracellular matrix. *Cell Mol Life Sci* 57(1):41–64.
38. Théry M, et al. (2006) Anisotropy of cell adhesive microenvironment governs cell internal organization and orientation of polarity. *Proc Natl Acad Sci USA* 103(52): 19771–19776.
39. Chon BH, Loeffler JS (2002) The effect of nonmalignant systemic disease on tolerance to radiation therapy. *Oncologist* 7(2):136–143.
40. Lin A, Abu-Isa E, Griffith KA, Ben-Josef E (2008) Toxicity of radiotherapy in patients with collagen vascular disease. *Cancer* 113(3):648–653.
41. Pandya JA, et al. (2014) Post-radiation changes in oral tissues: An analysis of cancer irradiation cases. *South Asian J Cancer* 3(3):159–162.
42. Stone HB, Coleman CN, Anscher MS, McBride WH (2003) Effects of radiation on normal tissue: Consequences and mechanisms. *Lancet Oncol* 4(9):529–536.
43. Baumketner A (2014) Electric field as a disaggregating agent for amyloid fibrils. *J Phys Chem B* 118(50):14578–14589.
44. Li M, et al. (2013) Photodegradation of β -sheet amyloid fibrils associated with Alzheimer's disease by using polyoxometalates as photocatalysts. *Chem Commun* 49(6):11394–11396.
45. Li M, Yang X, Ren J, Qu K, Qu X (2012) Using graphene oxide high near-infrared absorbance for photothermal treatment of Alzheimer's disease. *Adv Mater* 24(13): 1722–1728.
46. Soto C, et al. (1998) β-sheet breaker peptides inhibit fibrillogenesis in a rat brain model of amyloidosis: Implications for Alzheimer's therapy. *Nat Med* 4(7):822–826.
47. Li M, et al. (2013) Cerium oxide caged metal chelator: Anti-aggregation and anti-oxidation integrated H2O2-responsive controlled drug release for potential Alzheimer's disease treatment. *Chem Sci (Camb)* 4(97):2536–2542.